Improving estimates of the ionosphere during geomagnetic storm conditions through assimilation of thermospheric mass density

FernandezGomez, Isabel ; Kodikara, Timothy; Borries, Claudia; Forootan, Ehsan; Goss, Andreas ; Schmidt, Michael; Codrescu, Mihail V.

Published in:
Earth, Planets and Space

DOI (link to publication from Publisher):
10.1186/s40623-022-01678-3

Publication date:
2022

Document Version
Publisher's PDF, also known as Version of record

Fernandez-Gomez *et al.*
Earth, Planets and Space (2022) 74:121
https://doi.org/10.1186/s40623-022-01678-3

Earth, Planets and Space

FULL PAPER

Open Access

Improving estimates of the ionosphere during geomagnetic storm conditions through assimilation of thermospheric mass density

Isabel Fernandez-Gomez[1*], Timothy Kodikara[1], Claudia Borries[1], Ehsan Forootan[2], Andreas Goss[3], Michael Schmidt[3] and Mihail V. Codrescu[4]

Abstract

Dynamical changes in the ionosphere and thermosphere during geomagnetic storm times can have a significant impact on our communication and navigation applications, as well as satellite orbit determination and prediction activities. Because of the complex electrodynamics coupling processes during storms, which cannot be fully described with the sparse set of thermosphere–ionosphere (TI) observations, it is crucial to accurately model the state of the TI system. The approximation closest to the true state can be obtained by assimilating relevant measurements into physics-based models. Thermospheric mass density (TMD) derived from satellite measurements is ideal to improve the thermosphere through data assimilation. Given the coupled nature of the TI system, the changes in the thermosphere will also influence the ionosphere state. This study presents a quantification of the changes and improvement of the model state produced by assimilating TMD not only for the thermosphere density but also for the ionosphere electron density under storm conditions. TMD estimates derived from a single Swarm satellite and the Coupled Thermosphere Ionosphere Plasmasphere electrodynamics (CTIPe) physics-based model are used for the data assimilation. The results are presented for a case study during the St. Patricks Day storm 2015. It is shown that the TMD data assimilation generates an improvement of the model's thermosphere density of up to 40% (measured along the orbit of the non-assimilated Swarm satellites). The model's electron density during the course of the storm has been improved by approximately 8 and 22% relative to Swarm-A and GRACE, respectively. The comparison of the model's global electron density against a high-quality 3D electron density model, generated through assimilation of total electron content, shows that TMD assimilation modifies the model's ionosphere state positively and negatively during storm time. The major improvement areas are the mid-low latitudes during the storm's recovery phase.

Keywords: Data assimilation, Geomagnetic storm, Neutral density, Thermosphere–ionosphere system

*Correspondence: Isabel.FernandezGomez@dlr.de

[1] Institute of Solar-Terrestrial Physics, German Aerospace Center, Kalkhorstweg 53, 17235 Neustrelitz, Germany
Full list of author information is available at the end of the article

Graphical Abstract

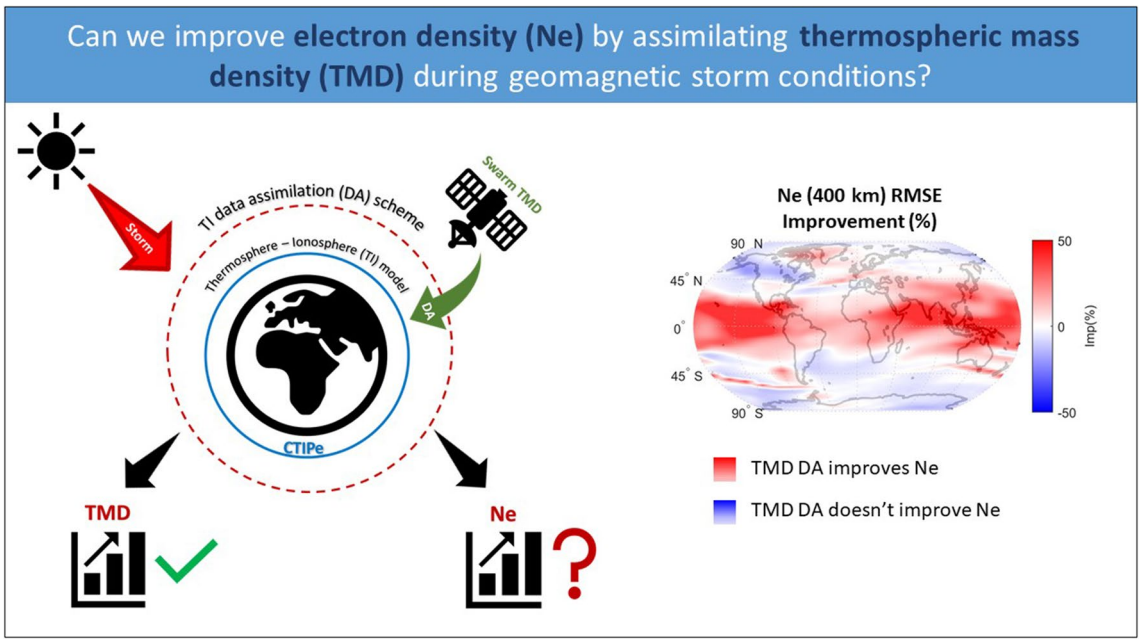

Introduction

The Earth's thermosphere (from 90 to 600 km altitude) is characterized by high temperatures generated by the absorption of solar ultraviolet irradiance. This absorption process causes partial ionization of the upper atmosphere, creating the ionosphere at that same altitude. The ionosphere describes the charged component of this system. Even though the density of the upper atmosphere is low, it has a significant impact on the trajectories and degradation of spacecrafts orbiting at those altitudes. The ionosphere's electron density is also an important parameter because it is critical for communications and navigation applications due to its direct relationship with radio wave transmission. For these reasons, it is vital to understand and monitor the state of the thermosphere–ionosphere (TI) system and its response to external drivers.

The TI is a coupled system, which means that the thermosphere state strongly influences the dynamics and electrodynamics of the ionosphere. Likewise, processes of electrodynamic nature that take place in the ionosphere feed back onto the dynamics of the thermosphere. Collisions in the upper atmosphere between neutral and charged particles constitute one of the mechanisms that couple the TI system dynamics. Neutral dynamics are influenced by collisions with ions and thermosphere winds have a strong effect on the ionosphere dynamics (Richmond and Roble 1997). In the event of strong solar transients passing Earth (e.g., coronal mass ejection or corotating interaction regions), large amounts of energy can be deposited in the upper atmosphere, generating dramatic changes in the TI system. This causes significant heating of the thermosphere, thermosphere expansion, changes in composition and electric fields and disturbance storm time neutral winds. As a consequence, increases (decreases) of electron density and TEC, i.e., positive (negative) storms occur in the ionosphere (Richmond and Roble 1997; Buonsanto 1999; Förster and Jakowski 2000).

Because TI observations have only sparse temporal and spatial coverage, physics-based models are essential to reproduce the TI state. Nevertheless, a few limitations of physical models lead to inaccuracies in the upper atmosphere representation that need to be considered. First, the hydrostatic balance between gravitational forces and vertical pressure gradients, used as a key assumption for most of them, is sufficient under most conditions, but during geomagnetic storms, this approximation has been proven to underestimate the thermosphere density response to the rapid changes in energy input (Deng et al. 2008). The lack of helium in physical model simulations also affects its contribution to thermal conductivity, viscosity, specific heat as well as its contribution to the TMD (Emmert 2015). Also, lower atmosphere gravity waves are one of the major drivers of thermosphere density variability. Although the knowledge of lower thermosphere composition is crucial to determine the thermospheric

density (Fuller-Rowell 1995), physics-based models usually do not capture the complete coupling with the lower atmosphere, leading to errors in the thermosphere parameters simulations.

An important means for improving the representation of the upper atmosphere with physical models is data assimilation (DA). DA is a standard technique in which measurements are combined with the output of a model (Carrassi et al. 2018). There exist numerous examples of assimilating different observations into numerical models to improve the TI estimation and forecast. To give some examples: TMD from low earth orbiting satellites (Matsuo et al. 2012; Codrescu et al. 2018; Ren and Lei 2020; Sutton 2018; Forootan et al. 2022), thermospheric winds (Hsu et al. 2021; Hsu and Pedatella 2021), TEC (Chartier et al. 2016; Chen et al. 2016b; Scherliess et al. 2004; Solomentsev et al. 2014), electron density (Chen et al. 2016a; He et al. 2019; Kodikara et al. 2021), FUV [simulations by Fuller-Rowell et al. (2004); Cantrall et al. (2019)], thermosphere temperature (Laskar et al. 2021) and combinations [e.g., He et al. (2021); Pedatella et al. (2020)]. Because of the importance of an accurate representation of the ionosphere for communication and navigation systems, great attention has been given to data assimilation of electron density or TEC to improve the ionospheric state. During these studies, it has been pointed out that updating the neutral composition in data assimilation state vector is essential to improve the model representation of the electron density. This is of special importance when the conditions in the upper atmosphere change fast, like during storm periods (Chartier et al. 2013; Chen et al. 2016b). In addition, some studies like Forootan et al. (2022), evaluate the effects of TMD assimilation into the TI system. However, the impact of TMD DA on the global accuracy of the ionosphere electron density estimation during a major storm event has not been investigated or quantified yet. This will be the focal point for the studies presented here.

This research evaluates the impact of TMD assimilation on the ionospheric state estimation with focus on storm conditions. In the study, TMD observations derived from the Swarm-A satellite are assimilated into the physics-based Coupled Thermosphere Ionosphere Plasmasphere electrodynamics (CTIPe) model during the St. Patricks Day storm 2015. In order to assimilate data, the background model is coupled with the ensemble Kalman filter (EnKF) Thermosphere Ionosphere Data Assimilation scheme (TIDA) (Kalman 1960; Codrescu et al. 2018). The performance of the assimilation process on the TI system is measured by comparing the simulation results with independent measurements of TMD along the orbit of non-assimilated Swarm satellites and electron density measurements from Swarm and GRACE satellites. In addition, the global ionospheric impact of TMD assimilation is evaluated using electron density maps from high-quality estimates derived from a data-driven B-Spline electron density model (Liang 2017; Goss et al. 2019; Erdogan et al. 2020).

St. Patrick's Day storm 2015

Subject of this study is one of the major space weather events of the 24th solar cycle, the St. Patrick's Day geomagnetic storm 2015 (Kamide and Kusano 2015). It was generated by a coronal mass ejection (CME) associated with a flare and a series of radio bursts (Wu et al. 2016). The storm can be characterized by its geomagnetic activity index as illustrated by Fig. 1a, where 3 days are represented from 16 to 18 of March, a pre-storm quiet day, the main phase of the storm and the first part of the recovery phase. The disturbance storm time index (*Dst*) shows the sudden storm commencement at 0445 UTC on the 17 March. The main phase of the storm starts at 0730 UTC on that day, reaching a minimum of − 223 nT, which classifies it as a major storm (Gonzalez et al. 1994). The planetary 3-h averaged *Kp* index follows a similar evolution. On a scale from 0 to 9, values larger than 4 are considered storm time and a maximum of 8 defines a G4 severe storm according to NOAA space weather scales (Kunches and Viereck 2012). The recovery phase starts around 2245 UTC on 17 March, taking several days to return to pre-storm conditions.

The St. Patrick's Day storm 2015 resulted in storm time disturbances in the TI system. A positive ionosphere storm was detected in TEC during the storm main phase (Astafyeva et al. 2015; Borries et al. 2016; Nava et al. 2016) and the negative storm phase took place on the 18th March, the first day of the geomagnetic storm recovery (Nava et al. 2016). Positive and negative ionosphere storms occur at different regions and local times. The storm time ionospheric density variations have been explained by Astafyeva et al. (2015) to be essentially due to neutral composition changes.

Models and data

The background model CTIPe used in the assimilation scheme is a three-dimensional time-dependent physics-based numerical model that solves neutral and plasma dynamics over four coupled components: thermosphere, high latitude ionosphere, mid-low latitude ionosphere–plasmasphere and electrodynamics scheme (Fuller-Rowell et al. 1996; Millward et al. 1996). The global atmosphere has a geographic $2^\circ \times 18^\circ$ latitude, longitude resolution. In the vertical dimension, the thermosphere is divided into 15 pressure levels from the lower boundary at 1 Pa (~80 km), to a varying altitude above 400 km depending on geomagnetic

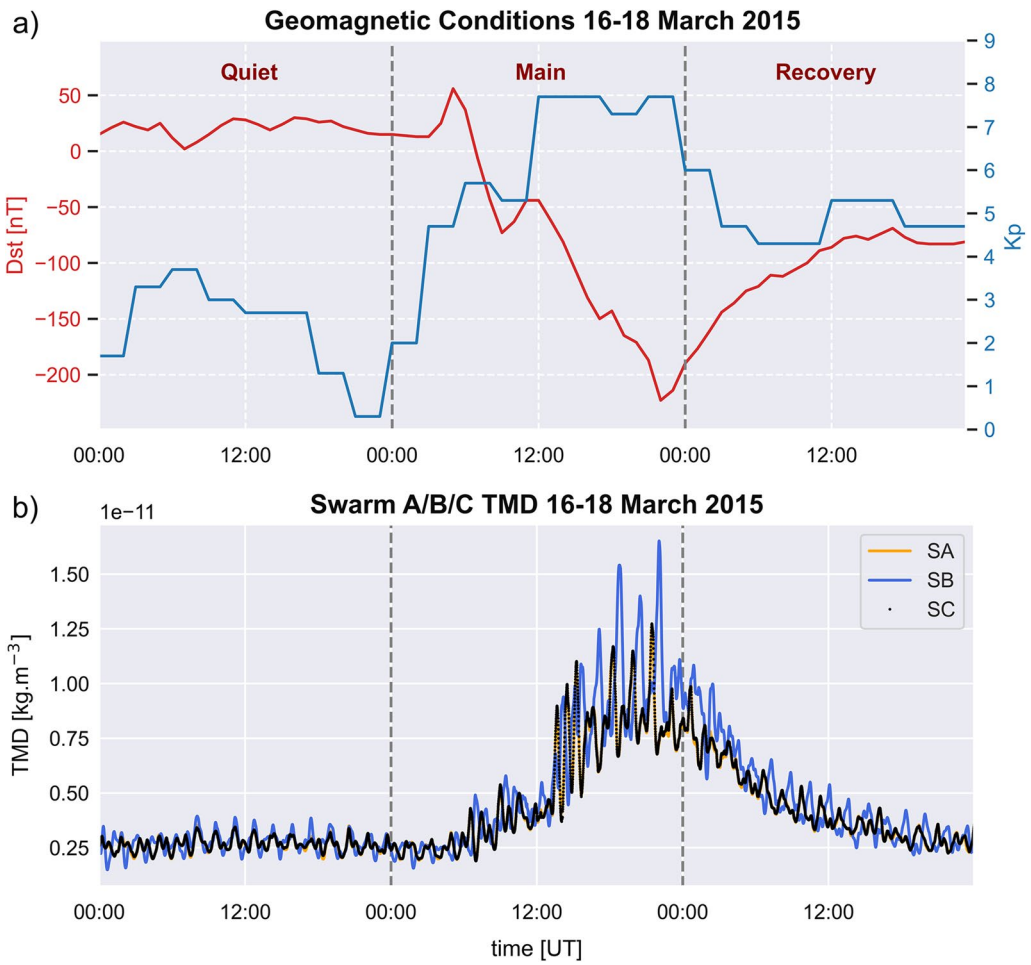

Fig. 1 St. Patrick's Day storm 2015. **a** geomagnetic activity represented by the *Dst* (red) and 3-h average *Kp* (blue) indices. **b** Along the orbit thermospheric mass density observations from Swarm-A, -B, and -C satellites (yellow, blue, and black) normalized to 400 km altitude. The period from 16 to 18 March 2015 includes a pre-storm quiet day, the main phase of the storm and the first day of the recovery phase. A strong perturbation in geomagnetic activity and neutral density is visible during the main phase of the storm

conditions. The magnetospheric input is built on an auroral precipitation statistical model described by Fuller-Rowell and Evans (1987) and electric fields by Weimer (2005). The auroral precipitation uses a hemispheric power index, based on TIROS/NOAA auroral particle measurements. To calculate dissociation, heating and ionization rates, a weighted average $F_{10.7}$ cm radio flux is included. Solar wind parameters from the Advanced Composition Explorer (ACE) are input of the model, namely solar wind speed $|v_{sw}|$, solar wind density ρ_{sw} and interplanetary magnetic field components (B_N, B_θ). At the lower boundary of 80 km, the model uses a simplified version of the Whole Atmosphere Model (Akmaev 2011). Its influence is then determined from a climatological run of the atmospheric forcing given by hourly averaged neutral temperature, zonal (east–west) and meridional (north–south) winds.

An implementation of an ensemble Kalman filter (EnKF), the Thermosphere Ionosphere Data Assimilation scheme (TIDA), is used to assimilate neutral mass density into the CTIPe model (Codrescu et al. 2018). The system updates following the Kalman filter equations (Kalman 1960) and three components can be differentiated: (1) the forecast state estimate or prior, (2) the analysis estimate of the state considering all measurements, and (3) a reference member run in parallel with no assimilation used to compare and measure improvement due to DA. Because of the strongly forced nature of the TI system (Huba et al. 2014) in combination with the large uncertainties associated with the external forcing (Pedatella et al. 2018; Fernandez-Gomez et al. 2019), the

EnKF state vector updates at each time step the model forcing parameters along with the model state (Eq. 1). Included in the update of the model forcing are the $F_{10.7}$ radio flux, the solar wind velocity and density, and the interplanetary magnetic field. The model state consists of all necessary parameters to calculate neutral density, i.e., mass mixing ratios for molecular nitrogen, atomic and molecular oxygen ($\gamma_O, \gamma_{O_2}, \gamma_{N_2}$), mean molecular mass M, zonal–meridional wind components (U, V) and neutral temperature T_n. TIDA specification is based on a special member, which means that there is an ensemble member whose forcing is the mean of the distribution from which the ensemble member forcing is sampled. The thermospheric true state of the system is approximated using this special member:

$$x = \left[(F_{10.7}, |v_{sw}|, \rho_{sw}, B_N, B_\theta);\ (T_n, \gamma_O, \gamma_{O_2}, \gamma_{N_2}, M, U, V)\right]. \tag{1}$$

TMD products derived from the European Space Agency (ESA) Swarm mission (Siemes et al. 2016) are used as observation during our experiment. The Swarm mission consists of three satellites A, B, and C. The Swarm-A and -C satellites fly side-by-side at an altitude of approximately 463 km (March 2015) and 87.35° inclination. Swarm-B orbits at an altitude of approximately 510 km with an inclination of 87.75°. The local time difference between Swarm-B and the Swarm-A–C pair is approximately 1.5 h. The precise orbit determination (POD) based on TMD estimates from Swarm-A with the temporal resolution of 30 seconds is used within the assimilation (Visser et al. 2013). The TMD is normalized to the common altitude of 400 km to minimize extrapolation problems due to the altitude differences within the assimilation period. For normalization, we used the vertical profiles from the NRLMSISE00 model (Picone et al. 2002) as described in Forootan et al. (2021), following Eq. 2. Where ρ is the density of Swarm and if ρ_N that of NRLMSISE00. The argument h is the altitude in km. The TMD estimates from Swarm-B and C data (normalized to 400 km altitude) are applied for validating the DA results. Fig. 1b shows an overview of the three Swarm satellite normalized neutral density observations during the quiet period before the storm (16 March), the drastic density increase that characterizes the storm time is visible around the 17th (main phase), and the start of the recovery phase the following day (18 March):

$$\rho(400) = \frac{\rho(h) * \rho_N(400)}{\rho_N(h)}. \tag{2}$$

The electron density estimates generated with this DA run are validated at different altitudes using electron density estimates obtained from different sources. First, along-track electron density from Swarm Electric Field Instrument (EFI) Langmuir Probes (Lomidze et al. 2018) are used to evaluate the change of electron density due to DA of TMD along the orbit of the assimilated satellite. Second, GRACE (Gravity Recovery and Climate Experiment) K-Band Ranging System (Xiong et al. 2021) is used to measure the change of electron density along the orbit of an independent satellite. GRACE is composed of two satellites, with 89° inclination and an initial altitude of about 490 km (403 km during March 2015). The K-Band Ranging System instrument along with Global Positioning System (GPS) Navigation data can provide TEC measurements and the position of the two satellites, allowing to derive the average electron density between them.

The B-Spline electron density model is used to measure the DA impact on the ionosphere on the global scale. It is developed at DGFI-TUM and based on the so-called multi-layer Chapman approach:

$$\begin{aligned} N_e(h) &= N_e^D(h) + N_e^E(h) \\ &\quad + N_e^{F_1}(h) + N_e^{F_2}(h) + N_e^P(h) \\ &= \sum_Q N_e^Q(h) + N_e^P(h), \end{aligned} \tag{3}$$

where the elements D, E, F_1, F_2 of the set $Q = \{D, E, F_1, F_2\}$ and P refer to the $D-$, $E-$, F_1- and F_2 -layer of the ionosphere as well as to the plasmasphere (Liang 2017). Each Chapman function $N_e^Q(h)$ describes approximately the vertical electron density distribution of the Q-layer. Herein, the three quantities, N_m^Q(= maximum electron density value), h_m^Q(= peak height) and H^Q(= scale height) are defined as the key parameters of the Q-layer. In addition, the function $N_e^P(h)$ describes the electron density distribution within the plasmasphere by means of the two key parameters N_0^P(= basis density of the plasmasphere) and H^P(= scale height of the plasmasphere). From these altogether 14 key parameters, the two most important ones, the peak value $N_m^{F_2}$ and the corresponding peak height $h_m^{F_2}$ of the F_2-layer, are modeled in two-dimensional (2-D) series expansions in terms of tensor products of 1-D endpoint-interpolating B-Splines depending on latitude φ and of 1-D trigonometric B-Splines depending on longitude λ (Goss et al. 2019). This way, the 1-D electron density representation $N_e(h)$ from (3) is transferred to the 4-D electron density model $N_e(\varphi, \lambda, h, t)$, where the time t means the fourth variable. Note, the other 12 key parameters are either assumed to be given or computable by simple formulae (Limberger et al. 2013). The unknown series coefficients of the B-Spline expansions are estimated from different input data sets. The first set is a VTEC product generated from GNSS (GPS, GLONASS) observations (Goss et al. 2019). These VTEC data or VTEC maps

$VTEC(\varphi, \lambda)$ are transferred to electron density observations $N_e(\varphi, \lambda, h) = VTEC(\varphi, \lambda) \cdot \bar{N}_e(h)$ according to the so-called separability approach (Hernández-Pajares et al. 1999) by introducing the normalized profile function $\bar{N}_e(h)$ with $\int_h \bar{N}_e(h)dh = 1$ calculated from the IRI 2012 model. The second data set includes additional GPS observations from IGS stations not considered in the generation of the VTEC maps. Since the unknown series coefficients of the B-Spline expansions are computed via a Kalman filter (Erdogan et al. 2020) with a temporal step size of 10 minutes, the estimated 4-D electron density model values $\widehat{N}_e(\varphi, \lambda, h, t_i)$ are provided at discrete time moments t_i with the same temporal resolution.

Methods

The characteristics of the assimilation experiment are the following:

- Swarm-A TMD observations normalized to the common altitude of 400 km are ingested into CTIPe model with the EnKF TIDA assimilation scheme from the 16th to the 18th March 2015.
- The days are classified in the study as: 16th the "quiet day", 17th the "main phase", 18th the "recovery day", and we will refer as "storm" to the three days (Fig.1).
- The state vector (Eq.1) updates the forcing input parameters of the model in addition to the model state with all the necessary quantities to calculate neutral density.
- Due to the rapid changes that happen in the TI system during storm conditions, the experiment assimilates measurements in 10 minute intervals (Chen et al. 2016b).
- The TMD measurement uncertainty used is 10%.

To assess the changes that assimilation of TMD has in the TI system, we evaluate the differences between the analysis estimate (state with assimilation) and the reference (independent model run with no assimilation in it). The metrics used are the correlation coefficient and root mean square error (RMSE). The RMSE (Eq. 4) measures the average error performed by the model defined by the difference between the observations (Obs) and the model results (Mod), where N is the sample size. The lower the RMSE values, the better the fit of the model to the observations. We define the improvement (IMP) percentage based on the RMSE of analysis (a) and reference (r) difference as in Eq. 5. In this way, positive values translate into areas of improvement of the model with assimilation:

$$\mathrm{RMSE} = \sqrt{\frac{\sum (\mathrm{Obs} - \mathrm{Mod})^2}{\mathrm{N}}} \tag{4}$$

$$\mathrm{IMP}(\%) = \frac{(\mathrm{RMSE}_r - \mathrm{RMSE}_a)}{\mathrm{RMSE}_r} 100. \tag{5}$$

Results

In this section, we analyze the differences between the model reference and the analysis estimate for the TI system in order to measure the improvement of data assimilation in both regions, with special attention to the changes produced in the ionosphere.

Thermospheric impact

Figure 2 shows TMD normalized to 400km for the 3 days of the storm and the three Swarm satellites. Represented from top to bottom are Swarm-A (assimilated) and Swarm-B/C for validation. Observations (yellow), reference (red) and analysis (dark blue) are displayed. The effect of DA in the thermosphere is visible in the discrepancy between analysis and reference. The differences are maximized at the peak of the storm and during the recovery phase, reaching values of more than 2×10^{-12} kg.m^{-3}. Both model runs are not able to fully capture the storm onset and the effect of DA is not remarkable during "quiet" conditions. However, DA does make a difference during the main and recovery phases. The improvement of the TMD assimilation into the thermosphere is measured by comparing with observations of the non-assimilated orbits, the Swarm-B/C satellites. Figure 3 represents how the neutral density normalized to the assimilation altitude of 400 km of the reference and analysis results are compared with the observations. Panels a and b correspond to the regression results for Swarm-B and Swarm-C, respectively, during the 3 days of the storm. The change in the correlation coefficient in both satellites, goes from $R_r \sim 0.60$ for the reference to $R_a \sim 0.80$ for the analysis, indicating a stronger relationship with the observations in the assimilation estimate than the reference. To measure the upgrade in the thermosphere due to data assimilation, the "RMSE Improvement" definition in Eq. 5 is used. Panel c stands for the improvement results, separated by storm phases and satellite, Swarm-B in blue and Swarm-C in red. Similar values are found for both satellites, with a difference of approximately 5%. The evolution of increasing improvement in the storm phases goes from 18% during the quiet day to 59% during the recovery phase. The improvement for the whole storm is up to 40%.

Ionospheric impact

To assess if the assimilation of TMD has an impact in the ionosphere, we evaluate the changes in electron density at the assimilation altitude (400 km). The columns of

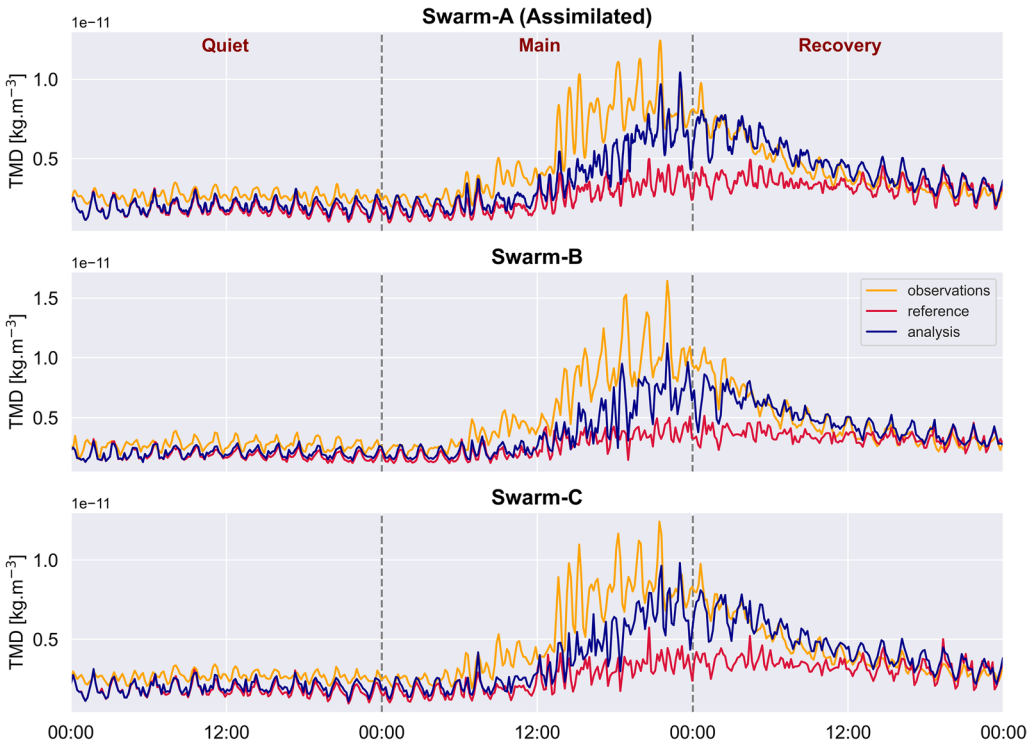

Fig. 2 Results of TMD normalized to 400km for Swarm-A (assimilated) and Swarm-B/C (validation). Observations (yellow), reference run (red) and analysis (blue) are shown for the 3 days 16–18 March 2015. The differences between reference and analysis during the main and recovery phases show the effect of data assimilation along the orbit of Swarm satellites. Differences up to 2×10^{-12} kg.m^{-3} are found during the peak of the storm

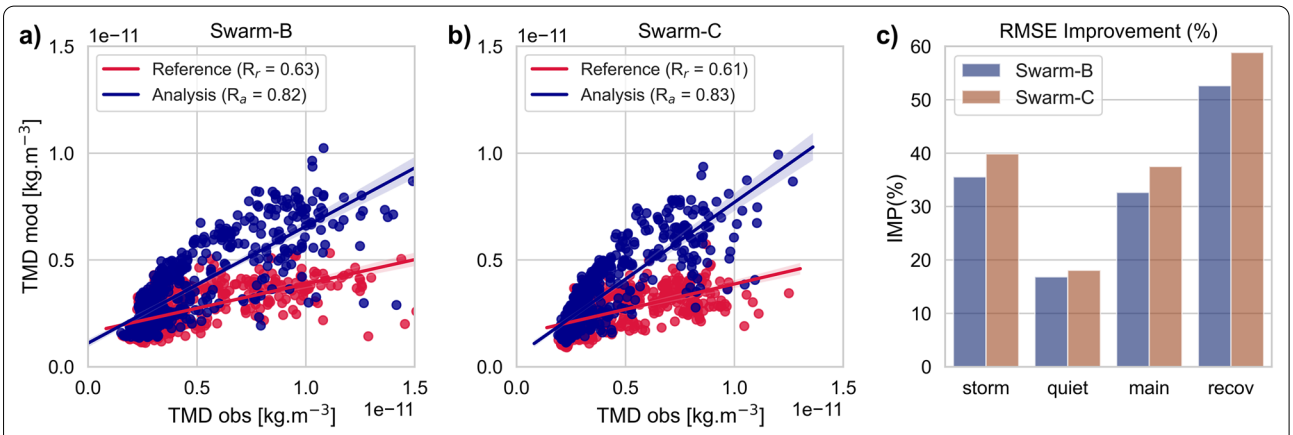

Fig. 3 Reference (red) and analysis (blue) regression against observations for normalized to 400 km thermospheric mass density results of **a** Swarm-B and **b** Swarm-C. The regression fit (straight line) is represented with its confidence interval (shadowed area). The correlation coefficient (R_r, R_a) improves from 0.6 to 0.8 in both satellites. The RMSE improvement (**c**) separated by storm phase and satellite (Swarm-B in blue and Swarm-C in red) exhibit an increase with the storm phases from 18% during the quiet day to 55% for the recovery phase

Fig. 4 represent the electron density maps of the reference run, the analysis estimate and the analysis - reference difference. The rows depict the phases of the storm (quiet, main phase and recovery) at 1200 UTC. The differences between analysis and reference are represented by a red–blue scale, indicating the discrepancy areas between the two model results. This demonstrates that data assimilation of neutral density has an impact on the ionosphere especially at mid and low latitudes. The location of the Swarm-A orbit track is also depicted (grey

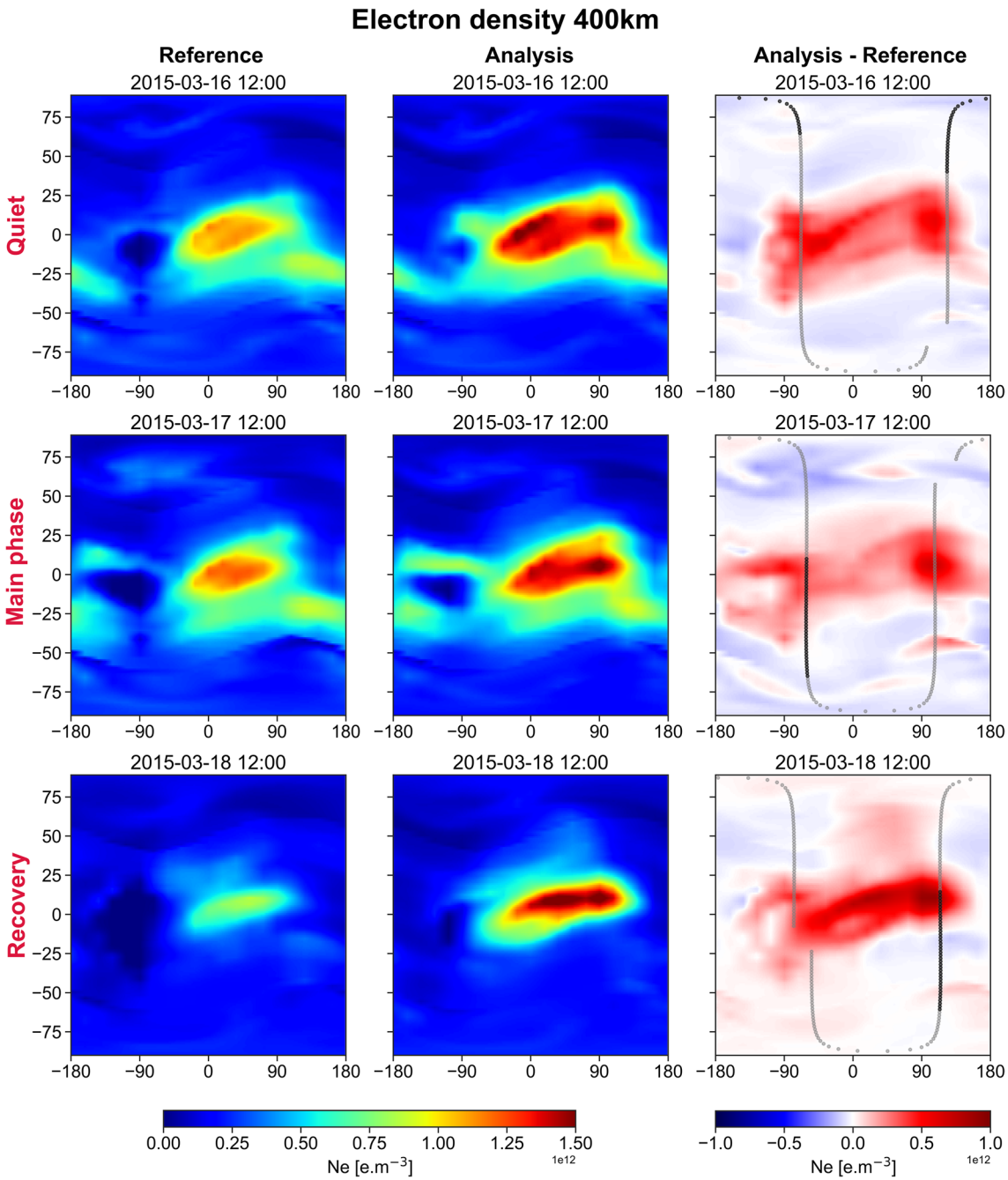

Fig. 4 Electron density maps at 400 km altitude for reference, analysis and analysis—reference difference at 1200 UTC (columns) during quiet, main phase and recovery days (rows). The location of Swarm-A orbit track is represented in the difference plot (grey line) with a highlighted area (black) of the last two assimilation intervals before 1200 UTC

line) with a highlighted area (black) representing the last two assimilation windows (20 min) of the satellite's path before 1200 UTC. The effect of the assimilation at different altitudes extends in a range from 200 km to 1000 km, finding the maximum differences between reference and analysis at mid-low latitudes around the assimilation altitude from 200 to 600 km (not shown here).

The electron density differences between reference run and analysis estimate show the impact of data assimilation in the ionosphere. However, to measure if those

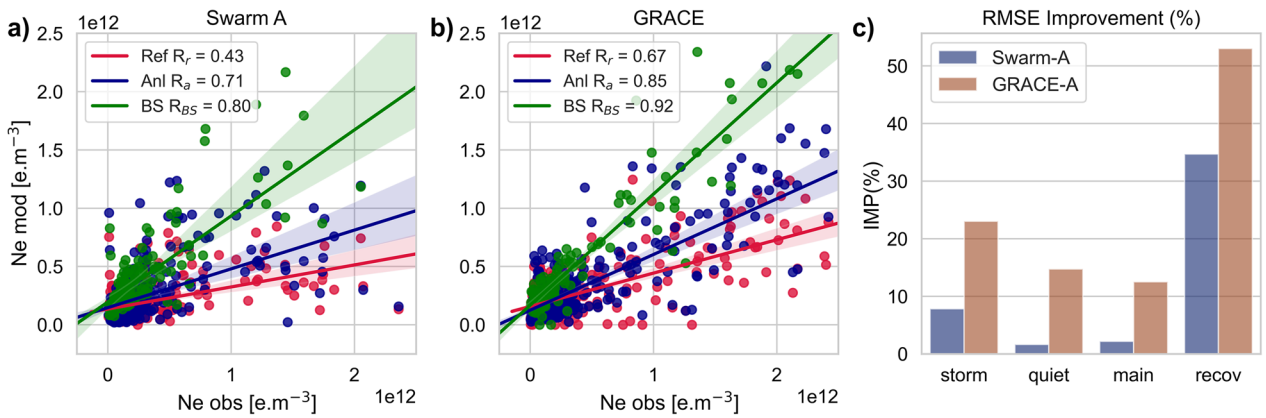

Fig. 5 Electron density reference (red), analysis (blue) and B-Spline model (green) regression against observations along the orbit **a** Swarm-A and **b** GRACE. The regression fit (straight line) is represented with its confidence interval (shadowed area). The correlation improves from reference to analysis in both cases and the B-Spline model exhibits a very strong correlation with the measurements. The RMSE improvement between reference and analysis separated by satellite and storm phases (**c**), shows the data assimilation upgrade increasing with the storm periods, with an average value of approximately 8% for Swarm-A and 22% for GRACE

changes are translated into an improvement of the ionosphere representation, we compare model results with electron density observations from along the orbit Swarm-A and GRACE satellites. The satellite measurements, in this case, are not normalized to 400 km in order to evaluate if the effect of data assimilation in the ionosphere extends along the satellite orbit altitude. The average altitude of the satellites at that time was 463 km for Swarm-A and 403 km for GRACE. The relationship between model results and observations for the three days of the storm is displayed in Fig. 5 for Swarm-A (a) and GRACE (b). Represented are: the reference (red), the analysis (blue) and the B-Spline model (green). The strength of the relationship between model and observations is measured by the correlation coefficient. A higher correlation with measurements is found for the analysis estimate (0.71 and 0.85), than for the reference (0.43 and 0.67), with a better adjustment with GRACE observations than with Swarm-A for reference and analysis. We can see how the RMSE improvement percentage evolves with storm phases in Fig. 5c. Swarm-A (blue) and GRACE (red) along the orbit improvement follow an analogous trend with the different storm periods, evolving from a very similar value during quiet and main phases to peak during the recovery phase. The storm improvement for the three days is 8% for Swarm-A and 22% for GRACE.

On the other hand, the B-Spline model exhibits a very strong correlation with observations (Fig. 5 a, b), confirming an accurate representation of the measurements with correlation coefficients of 0.80 and 0.92 for Swarm-A and GRACE, respectively. Therefore, the model results of the B-Spline electron density model are used to measure the global impact that the assimilation of one satellite orbit has on the ionosphere. The global electron density improvement map is calculated with respect to the electron density obtained with the B-Spline model. The improvement (Eq. 5) is obtained by calculating the RMSE of the electron density time series of each latitude and longitude point for the complete storm including quiet, main phase and recovery days. The results for the electron density at the assimilation altitude of 400 km are visible in Fig. 6, where the divergent red–blue scale represents positive–negative areas of improvement. In this context, "positive improvement" means areas where the RMSE of the reference is larger than the RMSE of the analysis. Therefore, at this altitude, the improvement of the assimilation is noticeable around the equatorial region between ±45° latitude (red). The average value of the positive improvement is 25%. Meanwhile the negative improvement areas (blue) where the reference run is better than the analysis estimate is 5%. The positive

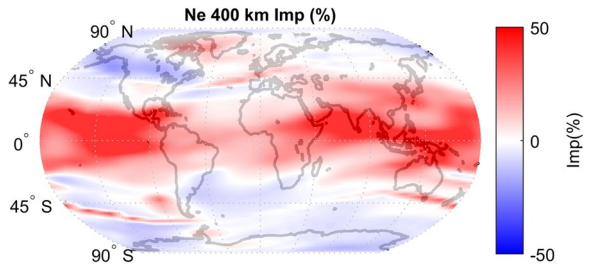

Fig. 6 Electron density global improvement at 400 km between analysis and reference with respect to the B-Spline model for the complete storm (quiet, main phase and recovery days). The main area of improvement (red) is around the equatorial area between (−45, 45)° latitude

effect of data assimilation extends to altitudes from 200 to 800 km (not shown here). For higher altitudes, the negative improvement areas become larger in extension and magnitude.

Discussion

According to Fig. 3c, the thermosphere is improved by the assimilation of neutral density. The correlation coefficient of observations against model results along the orbit of non-assimilated Swarm satellites (Fig. 3a, b), increases from a value 0.6 for the reference, to 0.8 for the analysis (see Table 1). The RMSE percentage improvement also increases depending on the storm phase with values that go from 15% for the quiet day to 55% for the recovery. Values of 35% improvement for the overall storm show the positive effect that data assimilation has on the model results. Therefore, during quiet time, the analysis estimate is not affected by the data assimilation as much as it is during the main and recovery phase (Fig. 2). However, the analysis run is not able to capture entirely the onset of the storm and the rapid changes that happen during the main phase, adjusting to the observations at the peak of the storm and once the recovery phase is reached. One of the reasons for the TIDA not following the real system at the beginning of the main phase of the storm, is that we have imposed limits on how much the forcing parameters are allowed to change from one assimilated time step to the next. This means that the response to the storm is artificially limited in TIDA at this time. The system forcing estimated as part of the Kalman state is not allowed to change from one assimilation time step to the next by more than the imposed values. The limits now in place were set for a quiet time, which could cause the filter to fall behind to rise in neutral density. In addition, there are some differences in the bias behavior depending on the storm phases, which is strongly negative during the quiet time but close to zero at the recovery phase. One possible explanation for this is that the uncertainty associated with the background model is state dependent, which means that it depends on the total amount of energy entering the TI system. The more energy entering the system, the larger the background model uncertainty and consequently, the larger the influence of measurements (considering constant uncertainty). The increase in background model uncertainty is caused by larger random variations in forcing assigned to the ensemble members when the state of the system is perturbed (when more energy is entering). This means that the model uncertainty is smaller during quiet times, reducing the influence of measurements. Based on this, we are making plans to find the optimum limits of the assimilation scheme that are expected to depend on many factors. The results of the optimization are planned to be presented in a future paper.

On the other hand, the differences in the electron density between reference and analysis (Fig. 4) demonstrate that TMD assimilation also has an impact on the ionosphere. The equatorial region is the most affected area at the assimilation altitude. Although the effects are seen in a range of heights between 200 and 1000 km, the largest differences are observed in a radius of 200 km around the assimilation height (400 km). Along with the differences, the orbit of the Swarm-A satellite centered at 1200 UTC is plotted, highlighting the position of the satellite in the last two assimilation windows before that time. It is observed that for the main and recovery phases, the satellite was close to the affected area. This is not the case for the quiet day. This is an indicator that the alterations produced in the ionosphere during storm phases are more affected by changes in neutral density than during quiet days.

We therefore compare the results with electron density measurements along the orbit of the Swarm-A and GRACE satellites (Fig. 5). The correlation coefficient between the model estimates with and without assimilating neutral density data, gives us a measure of the improvement in electron density in the ionosphere. It is also compared with the results for the B-Spline model to assess whether the fit of this model is appropriate for measuring the enhancement in the ionosphere on a global scale. In both cases, the lowest correlation coefficient is for the reference, followed by the analysis estimate and finally the B-Spline model, with better results for GRACE than for Swarm-A. This weaker fit of the model results with along the orbit Swarm-A electron density Langmuir Probes observations, could be

Table 1 Summary of TMD and electron density (Ne) correlation coefficient of reference (R_r) and analysis (R_a) and RMSE improvement (IMP) for along the orbit of different satellites observations

Satellite	Parameter	R_r	R_a	IMP_q (%)	IMP_m (%)	IMP_r (%)	IMP_s (%)
Swarm-B	TMD (400km)	0.63	0.82	18	32	52	35
Swarm-C	TMD (400km)	0.61	0.83	19	38	59	40
Swarm-A	Ne	0.43	0.71	2	3	33	8
GRACE	Ne	0.67	0.85	13	12	52	22

Improvement is separated by storm phases: quiet, main, recovery (*q*,*m*,*r*) and the complete storm (*s*)

explained by the systematic bias associated with these measurements that is translated in an underestimation of 10% in the plasma frequency and thus a 21% in the high electron density regions, as demonstrated by Lomidze et al. (2018). In addition, the altitude orbit of Swarm during storm time, was at 467 km, while GRACE was closer to the assimilation altitude at that time (403 km). The errors in the electron density estimation could also be due to the difference in height to the assimilation altitude of 400 km.

If we look at the results of the electron density RMSE improvement percentage (Fig. 5c), we see similar results for quiet time and the main phase of the storm. However, the effects of assimilating neutral density reach the maximum during the recovery phase, with a difference of more than 40% with respect to the quiet and main phase. According to Astafyeva et al. (2015), the positive ionospheric storm occurs during the main phase of the storm and the negative develops globally on March 18 at the beginning of the recovery phase. Negative storms can be explained mainly by the decrease in neutral density ratio O/N2, which results in an ion loss rate enhancement in the ionosphere. However, positive storm dynamics are influenced by factors other than changes in the thermospheric density, like thermospheric winds, prompt penetration or disturbance dynamo electric fields. In fact, Zhang et al. (2018) showed in a simulation study, that the neutral composition is the most important thermospheric parameter in ionospheric data assimilation and forecasts. This could explain the larger impact that the assimilation of neutral density has on the ionosphere during the recovery phase compared with the main phase.

The global map electron density improvement (Fig. 6) shows the positive effect of the assimilation around the equatorial region (±45°) at the assimilation altitude. This positive effect is limited at an altitude range between 200 and 800 km. Beyond that height, negative improvement areas become broader and increase their magnitude. A reason for that might be the fact that assimilating one orbit is not enough to constrain the neutral composition and, as a consequence, will not have a global impact on the ionosphere. Mass density variations can be produced by a change of height of the pressure level or a change in neutral composition, and unless the mass density assimilated is uniform and global coverage, it is not possible to distinguish the cause. In addition, data assimilation improves the model results "on average", which does not assure improvement of the thermosphere for all time periods, in which reference results can be better than the assimilated results. This could be the result of missing physics in the model, measurements with bias or with larger uncertainty than is used in the assimilation, or simply not enough or not ideally distributed measurements. In addition to these limitations, improving the representation of the ionosphere is a greater challenge with respect to data assimilation than neutral density, because the electron density depends not only on globally coherent neutral composition and temperature, but also on local neutral winds and electric field conditions. The correction of local conditions requires dense local data (winds) as well as electrodynamics conditions (Chen et al. 2016a).

Conclusions

In this study, thermospheric mass density from Swarm-A satellite is assimilated into the CTIPe physics-based model in order to improve the thermosphere–ionosphere system during the St. Patrick's Day storm 2015 and evaluate the effects of assimilating thermospheric parameters in the ionosphere. The correlation coefficient and RMSE percentage improvement with respect to observations are used to measure the differences between reference (without assimilation) and analysis (assimilation run) estimates of the TI system. The main results of this study can be summarized as follows:

- Neutral density improves along the orbit of the non-assimilated Swarm (B and C) satellites up to 40% over the three days considered in the study. The evolution of improvement is increasing with the different storm phases from the minimum during the quiet day with 15%, the main phase with 35% and finally the recovery phase with a maximum of 59%. The correlation coefficient of the model results against observations also shows an increase from 0.6 for the reference, to 0.8 for the analysis run.
- Electron density difference maps between reference and analysis show the effects of TMD DA at an altitude range of 200 to 800 km, demonstrating the influence of neutral density assimilation in the ionosphere.
- Electron density observations along the orbit of Swarm-A and GRACE satellites measure the improvement in the ionosphere, with better results for GRACE than for Swarm-A, with an overall value of 22% and 8%, respectively. The evolution with respect to storm phases shows a similar result for quiet time and main phase with low values in comparison with the recovery phase improvement.
- The global electron density improvement map depicts the areas that are affected by TMD assimilation. The positive effect extends over the equatorial region for all longitudes with an average improvement of 25%. The range of influence in altitude extends from 200

to 800 km. Beyond that value, negative improvement areas extend and increase in magnitude.

To conclude, we have demonstrated that the assimilation of neutral density measurements into a physics-based model during a major storm event is not only capable of correcting the thermosphere, but also of improving the global electron density estimates. The largest improvement in the electron density estimates has been identified in the equatorial region during the recovery phase of the storm.

Abbreviations

ACE: Advanced Composition Explorer; CTIPe: Coupled Thermosphere Ionosphere Plasmasphere electrodynamics model; CME: Coronal mass ejection; DA: Data assimilation; EnKF: Ensemble Kalman filter; GNSS: Global Navigation Satellite System; GLONASS: Globalnaja Nawigazionnaja Sputnikowaja Sistema; GPS: Global Positioning System; GRACE: Gravity Recovery and Climate Experiment; IGS: International GNSS Service; IRI: International Reference Ionosphere model; NRLMSISE00: US Naval Research Laboratory MSISE00; MSISE00: Mass Spectrometer and Incoherent Scatter radar Exosphere, year 2000; POD: Precise orbit determination; RMSE: Root mean square error; TEC: Total electron content; TI: Thermosphere–ionosphere; TIDA: Thermosphere Ionosphere Data Assimilation scheme; TMD: Thermospheric mass density; VTEC: Vertical total electron content.

Acknowledgements

The authors would like to thank the Swarm and GRACE missions for providing neutral and electron density data. Thanks to NASA OMNIWeb World Data Center, Kyoto University (Japan) and the German Research Centre of Geosciences for the Dst and Kp indices. We also wish to thank Mona Kosary from the University of Tehran for her assistance with the Swarm data normalization technique.

Author contributions

IFG designed the study, analyzed the data and wrote the manuscript. IFG, TK, CB and EF interpreted the results. EF provided the Swarm data normalized to the assimilation altitude. AG and MS contributed with the B-Spline electron density runs necessary for the validation of the results. MC helped with the discussion. CB is involved with acquisition of funding of the project. All the authors read, reviewed and approved the final manuscript.

Funding

Open Access funding enabled and organized by Projekt DEAL. This work was supported by the Insight II project from the German Research Foundation (DFG) with grant number BO 5011/2-2.

Availability of data and materials

The Swarm neutral mass density data assimilated in this study into the CTIPe model is stored at https://doi.org/10.5281/zenodo.6006365. Electron density from the Swarm mission can be found at (ftp://swarm-diss.eo.esa.int/) and GRACE at (ftp://isdcftp.gfz-potsdam.de/grace/). The Dst and Kp indices were provided by NASA OMNIWeb (https://omniweb.gsfc.nasa.gov/html/ow_data.html).

Declarations

Competing interests

The authors declare that they have no competing interests

Author details

[1]Institute of Solar-Terrestrial Physics, German Aerospace Center, Kalkhorstweg 53, 17235 Neustrelitz, Germany. [2]Geodesy and Earth Observation Group Institute of Planning, Aalborg University, Rendburggade 14, 9000 Aalborg, Denmark. [3]Deutsches Geodätisches Forschungsinstitut, Technical University of Munich, Arcisstrasse 21, 80333 Munich, Germany. [4]Space Weather Prediction Center, NOAA, 325 Broadway, 80305, Boulder, CO, USA.

Received: 10 February 2022 Accepted: 14 July 2022
Published online: 06 August 2022

References

Akmaev R (2011) Whole atmosphere modeling: connecting terrestrial and space weather. Rev Geophys. https://doi.org/10.1029/2011RG000364

Astafyeva E, Zakharenkova I, Förster M (2015) Ionospheric response to the 2015 St. Patrick's day storm: a global multi-instrumental overview. J Geophys Res Space Phys 120(10):9023–9037. https://doi.org/10.1002/2015JA021629

Borries C, Mahrous AM, Ellahouny NM, Badeke R (2016) Multiple ionospheric perturbations during the Saint Patrick's Day storm 2015 in the European-African sector. J Geophys Res Space Phys 121(11):11333–11345. https://doi.org/10.1002/2016JA023178

Buonsanto MJ (1999) Ionospheric storms: a review. Space Sci Rev 88(3):563–601. https://doi.org/10.1023/A:1005107532631

Cantrall CE, Matsuo T, Solomon SC (2019) Upper atmosphere radiance data assimilation: a feasibility study for GOLD far ultraviolet observations. J Geophys Res Space Phys 124(10):8154–8164. https://doi.org/10.1029/2019ja026910

Carrassi A, Bocquet M, Bertino L, Evensen G (2018) Data assimilation in the geosciences: an overview of methods, issues, and perspectives. Wiley Interdiscip Rev Clim Change 9(5):e535. https://doi.org/10.1002/wcc.535

Chartier AT, Jackson DR, Mitchell CN (2013) A comparison of the effects of initializing different thermosphere-ionosphere model fields on storm time plasma density forecasts. J Geophys Res Space Phys 118(11):7329–7337. https://doi.org/10.1002/2013JA019034

Chartier AT, Matsuo T, Anderson JL, Collins N, Hoar TJ, Lu G, Mitchell CN, Coster AJ, Paxton LJ, Bust GS (2016) Ionospheric data assimilation and forecasting during storms. J Geophys Res Space Phys 121(1):764–778. https://doi.org/10.1002/2014JA020799

Chen C, Lin C, Matsuo T, Chen W (2016a) Ionosphere data assimilation modeling of 2015 St. Patrick's Day geomagnetic storm. J Geophys Res Space Phys 121(11):11–549. https://doi.org/10.1002/2015JA021787

Chen C, Lin C, Matsuo T, Chen W, Lee I, Liu J, Lin J, Hsu C (2016b) Ionospheric data assimilation with thermosphere-ionosphere-electrodynamics general circulation model and GPS-TEC during geomagnetic storm conditions. J Geophys Res Space Phys 121(6):5708–5722. https://doi.org/10.1002/2015JA021787

Codrescu S, Codrescu M, Fedrizzi M (2018) An ensemble Kalman filter for the thermosphere-ionosphere. Space Weather 16(1):57–68. https://doi.org/10.1002/2017SW001752

Deng Y, Richmond AD, Ridley AJ, Liu HL (2008) Assessment of the non-hydrostatic effect on the upper atmosphere using a general circulation model (GCM). Geophys Res Lett. https://doi.org/10.1029/2007GL032182

Emmert J (2015) Thermospheric mass density: a review. Adv Space Res 56(5):773–824. https://doi.org/10.1016/j.asr.2015.05.038

Erdogan E, Schmidt M, Goss A, Görres B, Seitz F (2020) Adaptive modeling of the global ionosphere vertical total electron content. Remote Sens 12(11):1822. https://doi.org/10.3390/rs12111822

Fernandez-Gomez I, Fedrizzi M, Codrescu MV, Borries C, Fillion M, Fuller-Rowell TJ (2019) On the difference between real-time and research simulations with CTIPe. Adv Space Res 64(10):2077–2087. https://doi.org/10.1016/j.asr.2019.02.028

Forootan E, Farzaneh S, Kosary M, Schmidt M, Schumacher M (2021) A simultaneous calibration and data assimilation (C/DA) to improve NRLMSISE00 using thermospheric neutral density (TND) from space-borne accelerometer measurements. Geophys J Int 224(2):1096–1115. https://doi.org/10.1093/gji/ggaa507

Forootan E, Kosary M, Farzaneh S, Kodikara T, Vielberg K, Fernandez-Gomez I, Borries C, Schumacher M (2022) Forecasting global and multi-level thermospheric neutral density and ionospheric electron content by tuning models against satellite-based accelerometer measurements. Sci Rep 12(1):1–19

Förster M, Jakowski N (2000) Geomagnetic storm effects on the topside ionosphere and plasmasphere: a compact tutorial and new results. Surv Geophys 21(1):47–87. https://doi.org/10.1023/A:1006775125220

Fuller-Rowell T (1995) The dynamics of the lower thermosphere. Up Mesos Low Thermosphere Rev Exper Theory Geophys Monogr Ser 87:23–36. https://doi.org/10.1029/GM087p0023

Fuller-Rowell T, Evans D (1987) Height-integrated Pedersen and Hall conductivity patterns inferred from the TIROS-NOAA satellite data. J Geophys Res Space Phys 92(A7):7606–7618. https://doi.org/10.1029/JA092iA07p07606
Fuller-Rowell T, Rees D, Quegan S, Moffett R, Codrescu M, Millward G (1996) A coupled thermosphere-ionosphere model (CTIM). STEP report 239
Fuller-Rowell T, Minter C, Codrescu M (2004) Data assimilation for neutral thermospheric species during geomagnetic storms. Radio Sci. https://doi.org/10.1029/2002RS002835
Gonzalez W, Joselyn JA, Kamide Y, Kroehl HW, Rostoker G, Tsurutani B, Vasyliunas V (1994) What is a geomagnetic storm? J Geophys Res Space Phys 99(A4):5771–5792. https://doi.org/10.1029/93JA02867
Goss A, Schmidt M, Erdogan E, Görres B, Seitz F (2019) High-resolution vertical total electron content maps based on multi-scale B-spline representations. Ann Geophys. https://doi.org/10.5194/angeo-37-699-2019
He J, Yue X, Wang W, Wan W (2019) EnKF Ionosphere and Thermosphere data assimilation algorithm through a sparse matrix method. J Geophys Res Space Phys 124(8):7356–7365. https://doi.org/10.1029/2019ja026554
He J, Yue X, Ren Z (2021) The impact of assimilating Ionosphere and Thermosphere observations on neutral temperature improvement: observing system simulation experiments using EnKF. Space Weather. https://doi.org/10.1029/2021sw002844
Hernández-Pajares M, Juan J, Sanz J (1999) New approaches in global ionospheric determination using ground GPS data. J Atmos Sol Terr Phys 61(16):1237–1247. https://doi.org/10.1016/S1364-6826(99)00054-1
Hsu CT, Pedatella NM (2021) Assessing the impact of ICON/MIGHTI Zonal and Meridional winds on upper atmosphere weather specification in a whole atmosphere data assimilation system: an observing system simulation experiment. J Geophys Res Space Phys. https://doi.org/10.1029/2021ja029275
Hsu CT, Pedatella NM, Anderson JL (2021) Impact of Thermospheric wind data assimilation on ionospheric electrodynamics using a coupled whole atmosphere data assimilation system. J Geophys Res Space Phys. https://doi.org/10.1029/2021ja029656
Huba JD, Schunk RW, Khazanov GV (2014) Modeling the ionosphere-thermosphere, vol 201. Wiley, Hoboken
Kalman RE (1960) A new approach to linear filtering and prediction problems. J Basic En 82(1):35–45. https://doi.org/10.1115/1.3662552
Kamide Y, Kusano K (2015) No major solar flares but the largest geomagnetic storm in the present solar cycle. Space Weather 13(6):365–367. https://doi.org/10.1002/2015SW001213
Kodikara T, Zhang K, Pedatella NM, Borries C (2021) The impact of solar activity on forecasting the upper atmosphere via assimilation of electron density data. Space Weather 19(5):e2020SW002,660,. https://doi.org/10.1029/2020SW002660
Kunches J, Viereck R (2012) NOAA improves space weather watch products. Space Weather. https://doi.org/10.1029/2012SW000838
Laskar FI, Pedatella NM, Codrescu MV, Eastes RW, Evans JS, Burns AG, McClintock W (2021) Impact of GOLD retrieved Thermospheric temperatures on a whole atmosphere data assimilation model. J Geophys Res Space Phys. https://doi.org/10.1029/2020ja028646
Liang W (2017) A regional physics-motivated electron density model of the ionosphere. PhD thesis, Technische Universität München
Limberger M, Liang W, Schmidt M, Dettmering D, Hugentobler U (2013) Regional representation of F2 Chapman parameters based on electron density profiles. Ann Geophys 31:2215–2227. https://doi.org/10.5194/angeo-31-2215-2013
Lomidze L, Knudsen DJ, Burchill J, Kouznetsov A, Buchert SC (2018) Calibration and validation of Swarm plasma densities and electron temperatures using ground-based radars and satellite radio occultation measurements. Radio Sci 53(1):15–36. https://doi.org/10.1002/2017RS006415
Matsuo T, Fedrizzi M, Fuller-Rowell TJ, Codrescu MV (2012) Data assimilation of thermospheric mass density. Space Weather. https://doi.org/10.1029/2012sw000773
Millward G, Moffett R, Quegan S, Fuller-Rowell T (1996) A coupled thermosphere-ionosphere-plasmasphere model (CTIP). In: Schunk RW (ed) STEP handbook on ionospheric models. Utah university, Salt lake city, pp 239–279
Nava B, Rodriguez-Zuluaga J, Alazo-Cuartas K, Kashcheyev A, Migoya-Orue Y, Radicella S, Amory-Mazaudier C, Fleury R (2016) Middle- and low-latitude ionosphere response to 2015 St. Patrick's Day geomagnetic storm. J Geophys Res Space Phys 121(4):3421–3438. https://doi.org/10.1002/2015JA022299
Pedatella N, Lu G, Richmond A (2018) Effects of high-latitude forcing uncertainty on the low-latitude and midlatitude ionosphere. J Geophys Res Space Phys 123(1):862–882. https://doi.org/10.1002/2017JA024683
Pedatella NM, Anderson JL, Chen CH, Raeder K, Liu J, Liu HL, Lin CH (2020) Assimilation of Ionosphere observations in the whole atmosphere community climate model with Thermosphere-Ionosphere EXtension (WACCMX). J Geophys Res Space Phys. https://doi.org/10.1029/2020ja028251
Picone J, Hedin A, Drob DP, Aikin A (2002) NRLMSISE-00 empirical model of the atmosphere: statistical comparisons and scientific issues. J Geophys Res Space Phys 107(A12):SIA–15. https://doi.org/10.1029/2002JA009430
Ren D, Lei J (2020) Evaluation of physics-based data assimilation system driven by neutral density data from a single satellite. Space Weather. https://doi.org/10.1029/2020sw002504
Richmond A, Roble R (1997) Electrodynamic coupling effects in the thermosphere/ionosphere system. Adv Space Res 20(6):1115–1124. https://doi.org/10.1016/S0273-1177(97)00754-0
Scherliess L, Schunk RW, Sojka JJ, Thompson DC (2004) Development of a physics-based reduced state Kalman filter for the ionosphere. Radio Sci. https://doi.org/10.1029/2002RS002797
Siemes C, Da Encarnação JDT, Doornbos E, Van Den Ijssel J, Kraus J, Pereštỳ R, Grunwaldt L, Apelbaum G, Flury J, Olsen PEH (2016) Swarm accelerometer data processing from raw accelerations to thermospheric neutral densities. Earth Planets Space 68(1):1–16. https://doi.org/10.1186/s40623-016-0474-5
Solomentsev D, Jacobsen KS, Khattatov B, Khattatov V, Cherniak Y, Titov A (2014) Ionosphere data assimilation capabilities for representing the high-latitude geomagnetic storm event in September 2011. J Geophys Res Space Phys. https://doi.org/10.1002/2014ja020248
Sutton EK (2018) A new method of physics-based data assimilation for the quiet and disturbed thermosphere. Space Weather 16(6):736–753. https://doi.org/10.1002/2017sw001785
Visser P, Doornbos E, van den IJssel J, Teixeira da Encarnação J, (2013) Thermospheric density and wind retrieval from Swarm observations. Earth Planets Space 65(11):1319–1331. https://doi.org/10.5047/eps.2013.08.003
Weimer D (2005) Improved ionospheric electrodynamic models and application to calculating Joule heating rates. J Geophys Res Space Phys. https://doi.org/10.1029/2004JA010884
Wu CC, Liou K, Lepping RP, Hutting L, Plunkett S, Howard RA, Socker D (2016) The first super geomagnetic storm of solar cycle 24: "The St. Patrick's day event (17 March 2015)". Earth Planets Space 68(1):1–12. https://doi.org/10.1186/s40623-016-0525-y
Xiong C, Lühr H, Stolle C (2021) GRACE Electron Density derived from the K-Band Ranging System. Potsdam : GFZ Data Services 0101. https://doi.org/10.5880/GFZ.2.3.2021.003
Zhang Y, Wu X, Hu X (2018) Effects of estimating the ionospheric and thermospheric parameters on electron density forecasts. Sci China Earth Sci 61(12):1875–1887. https://doi.org/10.1007/s11430-017-9251-4

Publisher's Note